Microchemical Journal 150 (2019) 104058

Contents lists available at ScienceDirect

Microchemical Journal

journal homepage: www.elsevier.com/locate/microc

Detecting trace of mercury ions in water using photoacoustic method enhanced by gold nanospheres

Qiaozhi He[a,c], Qian Zhang[b], Wenwu Cao[c,*], Ting Yin[b], Siwei Zhao[a], Xiaoqia Yin[a], Hui Zhao[a,*], Wei Tao[a,*]

[a] Department of Instrument Science and Engineering, Shanghai Jiao Tong University, Shanghai 200240, China
[b] Institute of Nano Biomedicine and Engineering, Shanghai Engineering Research Center for Intelligent Diagnosis and Treatment Instrument, Key Laboratory for Thin Film and Microfabrication Technology of the Ministry of Education, Department of Instrument Science and Engineering, Shanghai Jiao Tong University, 800 Dongchuan Rd, Shanghai 200240, China
[c] Department of Mathematics and Materials Research Institute, The Pennsylvania State University, University Park, PA 16802, USA

ARTICLE INFO

Keywords:
Gold nanospheres
Mercury ions detection
Photoacoustic method
ppt-level

ABSTRACT

A gold nanospheres (Au NSs)-enhanced photoacoustic (PA) system has been developed to detect parts per trillion (ppt)-level mercury ion (Hg^{2+}) in aqueous environments, which combines the advantages of the high sensitivity of PA detection and high extinction coefficient of Au NSs. 4-mercaptophenylboronic acid (MPBA) is used as the aggregation agent to detect Hg^{2+} by a designed PA system. Experimental results demonstrate a linear relationship between the amplitude of PA signals and logarithmic concentration of Hg^{2+} in the range of 10 pM-1 μM (R = 0.994). The detection limit of this Au NSs-enhanced PA system is 78 pM (16 ppt, S/N = 3) with a quick response time of 1 min. This method has excellent selectivity for Hg^{2+} over other heavy metal ions, alkali, and alkaline earth metal ions. The system is cost-effective and shows a great potential for quick detection of Hg^{2+} trace in water with very high sensitivity.

1. Introduction

Environmental contamination by heavy metal ions has aroused worldwide concern in recent decades. Hg^{2+} is one of the most common heavy metal ions on earth and highly toxic to the ecosystem [1]. Excessive mercury ions can lead to serious damage in the brain [2], kidney [3], central nervous [4], immune [5] and endocrine system [6]. The maximum allowable level (MAL) of inorganic mercury in surface water and ground water is 2.5 nM (0.5 μL) standardized by the World Health Organization [7]. Concerns over security of drinking water urge researchers to exploit effective and rapid assays to detect Hg^{2+} in aqueous solutions. Although standard detection methods of Hg^{2+} (e.g. inductively coupled plasma mass spectrometry (ICP-MS)) has high sensitivity in complex environments, their applications are limited by the operating condition, high cost, and test speed [8]. However, Hg^{2+} generally break out and spread in a sudden fashion [9]. Those approaches necessarily being performed in professional laboratories are not appropriate for rapid detection of Hg^{2+}. Rapid detection methods of Hg^{2+}, e.g., immunoassay [10], biochemical sensors [11] and electrochemical sensors [12], are limited in sensitivity and selectivity. Therefore, methods with high precision and high efficiency are urgently needed.

In recent years, surface-functionalized gold nanoparticles (Au NPs) are applied in a large number of highly sensitive and selective assays for Hg^{2+} detection [13-15]. Au NPs are considered as a crucial detecting probe because of their high extinction coefficient and colorimetric difference caused by the aggregation or anti-aggregation [16]. The Au NPs-assisted methods are more adaptable for different operating conditions. Once aggregating, the surface plasmon resonance (SPR) of Au NPs will be seriously affected, which results in a huge red-shift of absorption peaks. While the maximum absorption peak (MAP) moves from ~ 520 nm to ~ 650 nm, gold colloid will have a significant color change from ruby red to blue, which makes Au NPs suitable for *in vivo* [17] and *in vitro* [18] trace detection. Several researchers have made great progress in Au NPs-based detection of Hg^{2+}, using colorimetric [13], fluorescent [14] and surface-enhanced Raman scattering (SERS) [15] approaches. However, the colorimetric and fluorescent methods are seriously affected by scattering light, whereas high

abbreviations: Au NSs, Gold nanosheres; Au NPs, gold nanoparticles; PA, photoacoustic; MPBA, 4-mercaptophenylboronic acid; MAL, maximum allowable level; SPR, surface plasmon resonance; PADS, photoacoustic detecting system; DAC, data acquisition card; MAP, maximum absorption peak

* Corresponding authors.
E-mail addresses: dzk@psu.edu (W. Cao), huizhao@sjtu.edu.cn (H. Zhao), taowei@sjtu.edu.cn (W. Tao).

https://doi.org/10.1016/j.microc.2019.104058
Received 20 February 2019; Received in revised form 1 July 2019; Accepted 2 July 2019
Available online 16 July 2019

scattering is a typical characteristic of collids. Other approaches (e.g. SERS) need expensive and bulky devices. Recently, Liu et al. [19] have discovered MPBA as a new aggregation agent to detect Hg^{2+}. Taking advantage of the self-dehydration condensation of boronic acids and high affinity between thiolates and Hg^{2+}, the aggregation of Au NPs caused by MPBA is suppressed in the presence of Hg^{2+}. In this assay, complicated surface modification on Au NPs has been avoided. Furthermore, MPBA is cheaper and more available than other agents for Hg^{2+} detection, like oligonucleotides [20], fluorophore [21], or amino acids [22].

As a new type of detection method, PA method has been widely applied to biomedical imaging [23], tumor therapy [24], detection of gas [25], liquid [26, 27] and solid [28], *etc.* This method is based on the generation of ultrasonic waves (i.e., PA waves), transformed by light absorption of materials. The generation of PA waves is only related to light absorption and cannot be affected by the scattered light, which implies that the PA method has higher sensitivity than other optical-based methods and can be applied in more complex environment. Huang et al. introduced a novel PA imaging detection for Hg^{2+} using quaternary ammonium group-capped gold nanorods [29]. This method can obtain a linear relationship between the amplitude of PA signals and Hg^{2+} concentration (0–10 μM), which is much higher than the MAL of Hg^{2+}. They ignored the logarithmic range when Hg^{2+} concentration is less than 1 μM. Besides, their imaging system, complicated synthesis procedure and instability of gold nanorods increase the costs and difficulty for Hg^{2+} detection.

Here, a novel approach of ppt-level Hg^{2+} detection in aqueous environments based on Au NSs-enhanced PA system has been proposed. A PA detecting system (PADS) has been developed, and MPBA is taken as an aggregation agent to achieve ppt-level Hg^{2+} detection. Compared to the above-mentioned methods, our method offers several benefits, including: (1) high sensitivity due to the combination of PA method and Au NSs; (2) cost-effective setup compared to ICP-MS, SERS, *etc.*;(3) short detecting time and friendly operation condition; (4) simplicity of operation without any surface modification or complex synthesis; (5) highly sensitive for ppt-level Hg^{2+} detection.

2. Results and discussion

2.1. The photoacoustic detecting setup

In order to acquire PA signal of tested samples, a set of PADD had been built as illustrated in Fig. 1. The PADS was appropriate for the detection of all kinds of non-corrosive liquid. It consumed less than 1 mL of tested samples including Au NSs and other additives. It could generate high-intensive PA signals up to several volts by an acoustic transducer with impedance matching layer and amplifying the signal by a charge amplifier. The PADS consisted of four parts: (I) Pulsed laser generation unit, (II) laser intensity monitoring unit, (III) PA conversion unit and (IV) data acquisition unit. A beam of periodic pulsed laser irradiated in the sample placed in a miniature PA cell. The irradiated volume expanded and contracted in the PA cell after each pulse with a typical frequency, resulting in a series of acoustic waves (i.e. PA waves). The PA waves were transformed to electrical signals by a highly sensitive piezoelectric transducer, and further amplified by a charge amplifier, eventually acquired by the data acquisition unit.

The pulsed laser generation unit (I) was made of a function generator (Tektronix AFG310) and a Nd:YAG pulsed laser (STL1064QW-1mJ) with a frequency doubler. This unit generated a series of pulsed laser as the illuminating source to produce PA waves. The TTL trigger from function generator was sent to the controller of Nd:YAG laser, which generated a beam of pulsed laser in 1064 nm. The frequency doubler converted the laser to 532 nm, which was close to MAP of Au NSs, so that the 532 nm -pulsed-laser was appropriate for the detection of Au NSs. The pulse width was 9.2 ns, spot diameter was 0.8 mm and repetition frequency was 100 Hz.

The laser intensity monitoring unit (II) included a 532 nm beam splitter prism and a silicon photocell, in order to remove the effect of laser intensity fluctuations on PA values. The laser was split into two beams by a beam splitter prism. One beam illuminated the PA conversion unit directly, as mentioned above, the other one was sent to silicon photocell to monitor the laser intensity and trigger the data acquisition card (DAC).

As the core component of the PADS device, the PA conversion unit (III) was composed of a customer made ultrasonic transducer and a miniature PA cell. The center frequency of the transducer was 0.65 MHz, which was close to theoretical frequency peak calculated by Lai's theory [30]. The ultrasonic transducer was coupled with a layer of epoxy resin to match the liquid impedance. PZT-5A was chosen as the piezoelectric material, which had higher piezoelectric coefficient to convert the acoustic signals into electrical signals [31]. The miniature PA cell was made of a micro cuvette (1 mL), the bottom of which was removed and directly glued on to the surface of ultrasonic tranducer, which allowed the liquid to make direct contact with the transducer surface. This PA cell was enclosed by two thick side walls and two thin side walls. By this PA cell, very small amount (about 600 μL) of testing sample was consumed. As presented in Fig. 1, the 532 nm-pulsed-laser illuminated the PA cell close to the bottom through the thicker glass wall. We took the first acoustic signal as effective PA signal, since the latter signals might mix with a series of reflected acoustic signals. The sound generated from the PA cell was transformed by the piezoelectric transducer and collected by the data acquisition unit.

The data acquisition unit (IV) was composed of a dual-channel DAC (SPECTRUM,M2i.2031, 8-bit), a charge amplifier (FEMTO, HQA-15M-10T) and a voltage amplifier (FEMTO, HVA-200M-40-F). Before being acquired by DAC, the PA electrical signal was amplified by the charge amplifier (charge gain: 10 V /pC). In addition, the silicon photocell signal was amplified by the voltage amplifier (voltage gain: 20 dB). The sampling rate of DAC was up to 100 MS/s. The acquired data was saved in PC for further processing.

2.2. Sensing mechanism

A PA signal was generated from the conversion of absorbed optical energy into heat during the process of non-radiative transition [32]. When an intense pulsed laser irradiated on the plasmon of Au NSs, electrons of the conduction band would absorb photo energy and transfer it into heat in a few picoseconds [33]. A gold nanoparticle could absorb more than a thousand protons in a single laser pulse, increasing its temperature to reach the boiling point. When Au NSs were irradiated by periodical pulsed laser, the cylindrical illuminated zone would expand and contract with the same frequency, which gave rise to acoustic waves. The intensity of these acoustic waves was proportional to the absorption of Au NSs at the same wavelength, given by Eqs. (1) and (2) [30].

$$P_A = \frac{\alpha\beta}{C_P}\frac{\partial\Phi}{\partial t} \tag{1}$$

$$\left(\frac{1}{\upsilon_a^2}\frac{\partial^2}{\partial t^2} - \nabla^2\right)\Phi = I \tag{2}$$

where P_A represented the pressure of the acoustic wave, α was the optical absorption coefficient, β was volume thermal expansion coefficient, C_p was specific heat of the solution at constant pressure, υ_a was the sound velocity.

In order to accurately detect Hg^{2+} concentration, MPBA was taken as an aggregation agent, which induced Au NSs dispersing in the presence of Hg^{2+}. As depicted in Fig. 2, this method was based on the anti-aggregation of Au NSs by competition between Au NSs and aggregation agent–MPBA with Hg^{2+}. With the protection of negatively charged citrate ions, the Au NSs kept dispersed in aqueous solution. The electrostatic repulsion between Au NSs prevented them from aggregation,

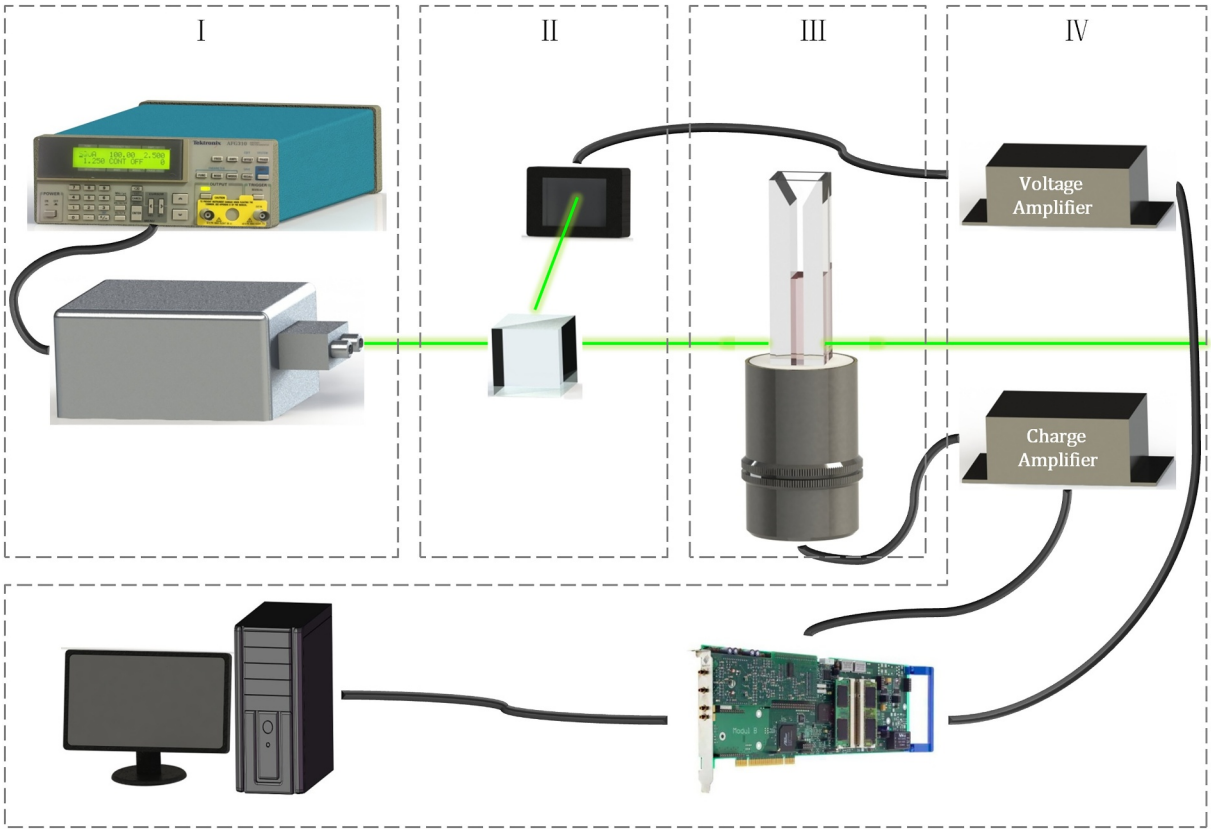

Fig. 1. The setup of the PADS, including (I) Pulsed laser generation unit, (II) laser intensity monitoring unit, (III) PA conversion unit and (IV) data acquisition unit.

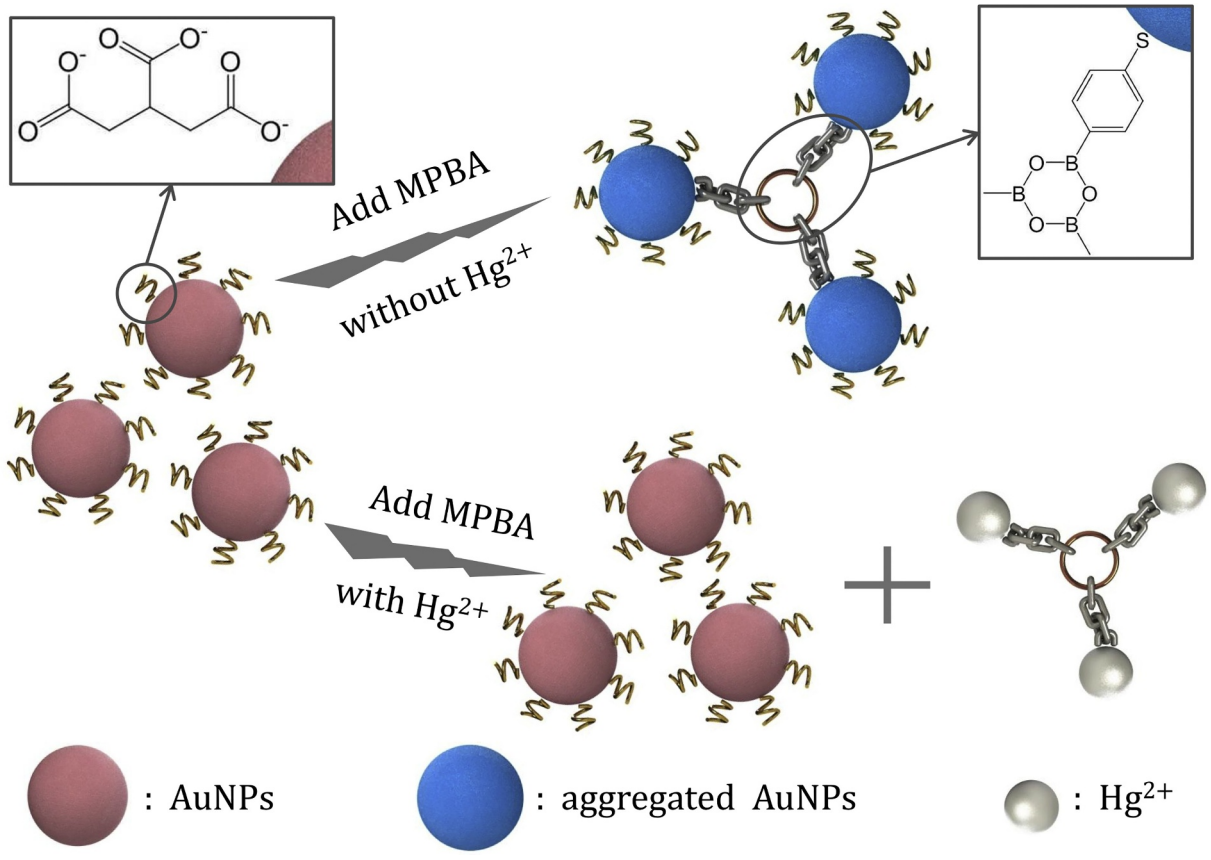

Fig. 2. A schematic mechanism of sensing Hg^{2+} based on anti-aggregation of Au NSs and high affinity between thiolates and MPBA.

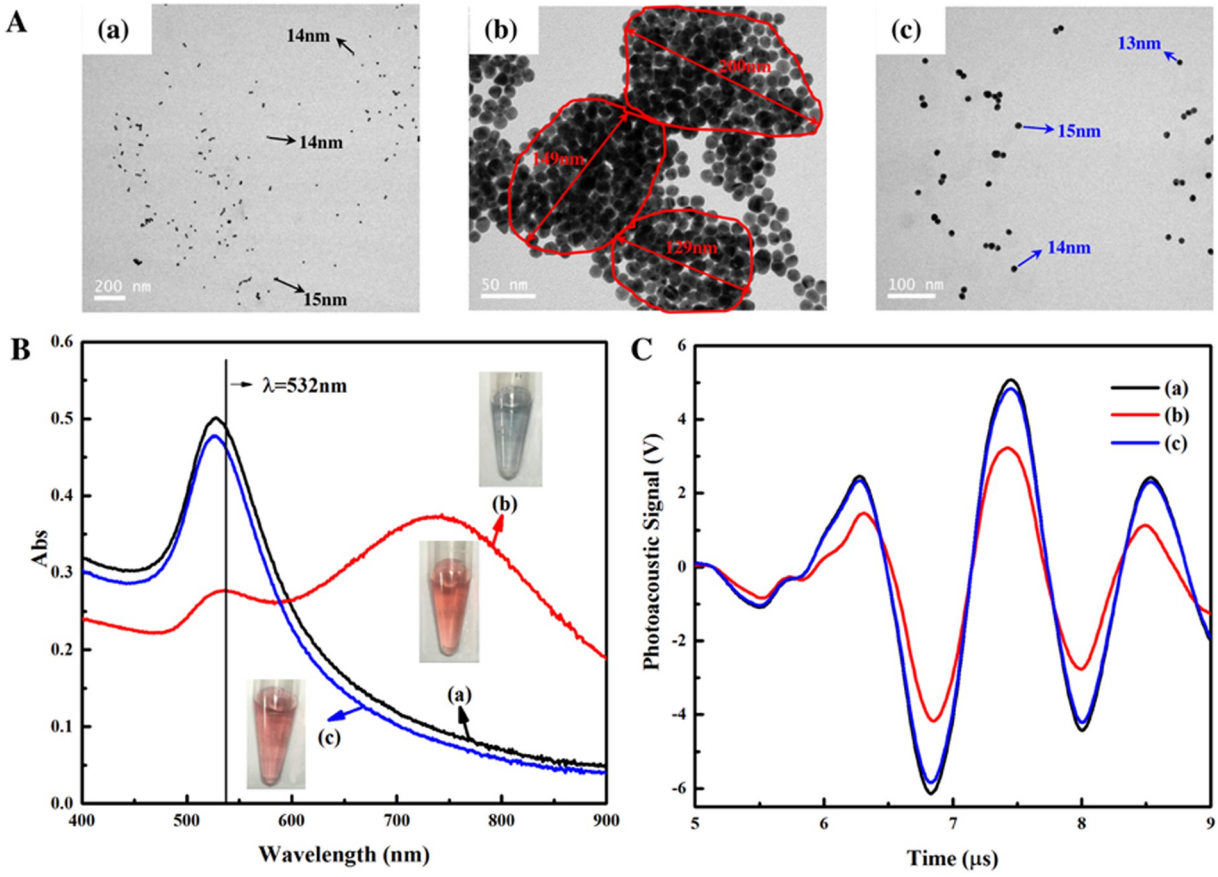

Fig. 3. (A) TEM, (B) UV-Vis spectra and (C) original PA signal diagram of Au NSs solution (a), and MPBA-Au NSs solution (b) and 1μM Hg^{2+} (c).

and the solution showed ruby red. A MPBA molecule had two hydroxyl groups which were unstable in aqueous environment. As a consequence, three MPBA molecules could form a boroxine ring by eliminating three water molecules [34]. The MPBA had the ability of connecting with Au NSs because of specific Au-S interaction. Au NSs were grasped together in the presence of MPBA, which was described as chain links in Fig. 2.

This interaction resulted in a visible color change of gold colloid from ruby red to blue, corresponded to a red-shift of absorption band. However, if MPBA was mixed with Hg^{2+} in advance, the aggregation would decrease as high binding affinity between thiolates and Hg^{2+} inhibited the binding of thiol group with Au NSs. In this case, MPBA was incapable of attaching to the surface of Au NSs and making Au NSs aggregate. As the Hg^{2+} concentration increased, the color of the mixed solution changed from blue to ruby red. This indicated that the aggregated Au NSs re-dispersed into the solution. The anti-aggregation of Au NSs induced by Hg^{2+} was further verified by TEM images and UV-Vis absorption spectra. As depicted in Fig. 3A, Au NSs aggregated after a 5.6 μL of MPBA (1 mM) was added, resulting from the self-dehydration condensation of boronic acid, and the size of Au NSs changed from 14 nm to 200 nm (Fig. 3A). When there were Hg^{2+} present, Au NSs were well dispersed because thiolates could form complexes with Hg^{2+} due to the high affinity and dropout from the surface of Au NSs. TEM images, UV-Vis absorption spectra and color changes in the absence and presence of 1 μM Hg^{2+} confirmed the mechanism. Consequently, this assay was suitable for Hg^{2+} detection and there is no need to add any masking agents. In addition, as shown by the blue arrow in Fig. 2C, excess Hg^{2+} would scramble for citrate ions which were intended to protect Au NSs, causing Au NSs to aggregate again.

The absorption at MAP (~ 520 nm) increased as Au NSs dispersed, which increased the intensity of PA waves accordingly. Benefit from the high extinction coefficient ($2.7 \times 10^8 Lmol^{-1}\ cm^{-1}$) of Au NSs [35], these PA waves could be detected by our PADS easily. PA signals were further amplified to more than 10 V peak to peak by a charge amplifier, which made our PADS more sensitive than traditional optical detection and this new method is suitable for ppt-level detection of Hg^{2+}.

2.3. Sensitivity of the Au NSs-enhanced PA system

To evaluate the sensitivity of Au NSs-enhanced PA system, samples containing various concentrations of Hg^{2+} from the same solution were detected using PADS. A pulsed laser (532 nm) was used as the illumination source, which meant that the acquired PA signal only reflected the absorption at 532 nm. Fig. S1B showed the original PA signals with different Hg^{2+} concentrations. Obviously, the amplitude of PA signal grew with the concentration of Hg^{2+} solution within the concentration of 10pM - 1μM. As shown in Fig. S1C, PA values (under λ = 532 nm) were defined by the ratio of the peak to peak value of PA signal (as marked by red arrow in Fig. S1B) over the laser intensity. The laser intensity was measured by the silicon photocell whose output was also voltage, which indicated that the measured PA value was a dimensionless value.

As the concentration of Hg^{2+} increases, more MPBA molecules will be linked with Hg^{2+} *via* thiol groups instead of Au NSs, which caused Au NSs to re-disperse. The color of Au NSs solution changed gradually from blue to purple, finally to ruby red. As shown in Fig. 3B, the MAP of Au NSs synthesized in this experiment was 521 nm, which strongly depended on the size of nanoparticles. The aggregation of Au NSs could be considered as a particle-size-increasing process for which the MAP of Au NSs was largely red-shifted and the intensity of MAP also changed. In the experiments, Nd:YAG pulsed laser was chosen in order to generate high-intensitive PA waves by increasing PA conversion efficiency.

As verified in Fig. 3B, the absorption of Au NSs in 532 nm increased greatly when the final Hg^{2+} concentration was (1μM) and Au NSs re-dispersed. Fig. 3C showed that the amplitude of PA signal increased significantly when the Hg^{2+} concentration reached 1μM. As a consequence, the amplitude of PA signals of Au NSs was expected to rise with the increase of Hg^{2+} concentration since Au NSs were changed from an aggregation to a dispersion condition.

As demonstrated in Fig. S1, the final Hg^{2+} concentration in sample solutions were between 10 pM and 10 μM. The relationship could be described by

$$y = 0.2337\log(x) + 2.6451 (R = 0.994) \quad (3)$$

where y denoted PA value defined by the ratio of the output amplitude of PA signal over the amplitude of the input voltage for the laser, both in volts, so that y is dimensionless; x denoted the concentration of Hg^{2+} in mol/L. The detection limit was 78 pM determined from the expression 3 S/K, where S was the standard deviation for 11 determinations of blank samples and K is the slope of the logistic regression model. The logistic regression model saturated at 1 μM, indicating that almost all of the thiol groups had connected with Hg^{2+} and Au NSs were totally dispersed. When the Hg^{2+} concentration was over 1 μM, the PA value declined due to the aggregation caused by Hg^{2+} itself. In contrast, the color change was indistinguishable by naked eyes at low Hg^{2+} concentration until the solution (1μM) totally changed to red, as shown in Fig. S1A, while clearly recognizable. More importantly, the sensitivity of naked eyes to color change varies from person to person. Furthermore, the detection limit of our PA system for Hg^{2+} is much lower than colorimetric method presented by Liu et al., which was 8 nM detected by an UV-2300 spectrophotometer (Shimadzu, Japan). In addition, the Au NSs-enhanced PA system will not be affected by scattering and reflection of laser, which meant our proposed method for Hg^{2+} can work even for complicated aqueous solution with ppt-level Hg^{2+} inclusion.

2.4. Optimum conditions

The main parameters which could affect the test result are the ratio between concentration of Au NSs and MPBA, reaction time, temperature, laser pulse width and power. The influence mechanism of these is interpreted as follows.

The concentrations of MPBA and Au NSs, or the ratio between them, is crucial for quantitative detection at low concentration. With too little MPBA, even if high concentration of Hg^{2+} is added in the mixture, the PA value could hardly change. In other words, a low sensitivity measurement would be obtained. On the contrary, if too much MPBA is added into Au NPs, Au NPs will completely aggregate and the initial PA value will be the lowest. In this case, highly sensitive measurement could be realized, because very low concentration of Hg^{2+} can change the PA value substantially. However, under this condition, STNR is too low for this Hg^{2+} trace measurement. Therefore, there is supposed to be a balance between the requirement of high sensitivity and high signal to noise ratio (STNR). In our experiment, the ratio between MPBA and Au NSs is chosen according to Zhou et al.'s work. Under such a condition, a highest ratio of signal to background can be obtained at the MPBA concentration of 10 μ M [36].

Fig. S2 showed the relationship between the amplitude of PA signals and Hg^{2+} concentration under different testing time. The initial time was set at the moment when gold colloid mixed with Hg^{2+} solution. The mixture concentration was determined by PADS with a time interval of 1–5 min in each addition of Hg^{2+}. Although the PA values existed differences at different times, they kept a great linear relationship with Hg^{2+} concentration. This makes it possible to shorten testing time within 1 min.

The peak photoacoustic pressure can be expressed by Eqs. (1), (2) and(4) [37].

$$P_A \approx \pm \frac{\beta I \alpha \upsilon_a^2}{2\pi C_p (\upsilon_a \tau_L)^{3/2} r^{1/2}} \quad (4)$$

where τ_L is the laser pulse width, r is the distance from irradiation center. According to these equations, the PA value has a negative relation with laser pulse width, while it is proportional to laser power. The pulsed laser incorporated in our designed detection system is Nd:YAG pulsed laser, which has a short pulse width of 9.2 ns. For this pulsed laser and most of the others, the pulse width is not accessible to be controlled. It is impossible for us to show the effect of pulse width by experiments. As for Eq. (4), the more intensive laser energy is, the higher signal-to-noise ratio we can obtain. However, the Acquiring range of DAC which is ± 5 V is considered in our experiments, which means the laser intensity cannot be too high.

2.5. Selectivity of the Au NSs-enhanced PA system

To figure out the selectivity of Au NSs-enhanced PA system for Hg^{2+} detection, other common metallic ions in aqueous environment, including Cd^{2+}, Cu^{2+}, Pb^{2+}, Fe^{3+}, Co^{2+}, Ni^{2+}, k^{+}, Mg^{2+}, Fe^{3+}, Ca^{2+}, Na^{+}, and Al^{3+} were also detected using our PADS for comparison.

The selectivity of PA system for Hg^{2+} detection was closely related to the high affinity between Hg^{2+} and thiolates. The reason why the binding affinity between thiolates with Hg^{2+} is higher than that of thiol groups with Au NSs could be interpreted by hard/soft acid/base(HSAB) principle presented by Ayers [38], who suggests that the formation of covalent bonds can be more stable and faster between molecules with similar hardness. Hg^{2+} had the characteristics of large radius, low positive charge and high polarizability. These were typical features of soft acids. Thiol groups also had high polarizability, small electronegativity and could be considered a soft base. According to the HSAB principle, a soft acid and soft base could be connected by covalent bonds, and eventually form a stable compound. Therefore, mercury ion had higher affinity than Au towards thiol group. It could replace the gold nanoparticle and to connect with thiol group easily. Other metal ions (hard acid) had lower affinity than mercury ion or Au so that they were difficult to induce the anti-aggregation of Au NSs in the presence of MPBA.

As illustrated in Fig. S3, upon adding the mixture of MPBA with each kind of metal ions (1 μM), only Hg^{2+}resulted in a remarkable increase of the PA amplitude, while other metal ions did not bring in noticeable enhancement. These test results verified that only Hg^{2+} had the ability of inducing anti-aggregation of Au NSs due to the high binding affinity between Hg^{2+} and thiolates. Other hard-acid metal ions, like k^{+}, Mg^{2+}, Fe^{3+}, Ca^{2+}, Na^{+}, Al^{3+}, were incapable of re-dispersing Au NSs. As a consequence, the colors of Au NSs solutions remained blue, only the one added Hg^{2+} turned into ruby red. Cd^{2+}, another typical soft acid, could also induce the aggregation of Au NSs but in a much smaller degree than Hg^{2+}. The property of Cu^{2+}, Pb^{2+}, Fe^{3+}, Co^{2+}, Ni^{2+}, were in between soft and hard acids. Therefore, our Au NSs-enhanced PA system demonstrated great selectivity for Hg^{2+} towards other metal ions.

Concentrations of Hg^{2+}, Cd^{2+}, Cu^{2+}, Pb^{2+}, Fe^{2+}, Co^{2+} and Ni^{2+} in drinking water is listed in Table S1. Concentrations between Hg^{2+} or other metal ion, taking Fe^{2+} as an example, may be more than 100 times different. In this case, it would not be possible to distinguish Hg^{2+} and Fe^{2+} by this proposed method. Nevertheless, this seems to be a common problem in detecting Hg^{2+} by gold nanoparticles [39-41].

Overall, this Au NSs-enhanced PA system has the benefit of high sensitivity and selectivity without any masking agents, and is potential for Hg^{2+} detection in practical situations.

2.6. Practical application

In order to test the Au NSs-enhanced PA system in natural water condition, tap water was used as a solvent to detect Hg^{2+} since it

includes multiple metal ions, like Ca^{2+}, Mg^{2+}, K^{+}, *etc.* Tap water was collected in our laboratory and spiked with a small amount of Hg^{2+} standard solution (100 μg mL^{-1}) to prepare Hg^{2+} solutions with different concentrations. The Hg^{2+} solutions were then measured and analyzed using our PA system. The results were displayed in Fig. S4.

The proposed PA system showed a clear logarithmic relationship between PA values and Hg^{2+} concentrations in tap water ($R = 0.982$). The test results had slight difference between Hg^{2+} detection in tap water and ultrapure water, possibly caused by the anionics and impurities in tap water. Despite this, the results indicated that this Au NSs-enhanced PA system is effective in Hg^{2+} detection for practical applications.

3. Conclusion

In summary, a highly sensitive Au NSs-enhanced PA system for ppt-level Hg^{2+} detection was developed, which combined the advantages of high sensitivity of PA detection and the extremely strong SPR absorption of Au NSs. The self-dehydration condensation of MPBA and higher affinity between thiol groups and Hg^{2+} was utilized to detect Hg^{2+} in aqueous solutions. The detection limit of this system reached 78 pM, which was much lower than the MAL of inorganic mercury in ground water. The sensitivity of the new PA system depended on the affinity between Au NSs and the aggregation agent, which was not limited to MPBA, indicating that the detection limit of Hg^{2+} could be further improved by substituting the aggregation agent with a better one. Furthermore, the high-resolution acoustic signal could be optimized by using better data processing algorithm and DAC with higher resolution. The PADS also demonstrated the applicability for Hg^{2+} detection in practical applications. In addition, it is far more cost-effective than ICP-MS, SERS or UV-Vis spectrophotometer and does not require complicated pretreatment. This system has great potential for routine detection and monitoring Hg^{2+} in aqueous environments.

4. Experimental section

4.1. Chemicals and reagents

Chloroauric acid trihydrate ($HAuCl_4 \cdot 3\,H_2O$) and MPBA were obtained from Shanghai Aladdin Bio-Chem Technology Co., Ltd. Sodium citrate (99%, anhydrous) and Citric acid (98%, anhydrous) were bought from J&K Chemical Ltd. (Shanghai, China). Hg^{2+} standard solution (100μg mL^{-1}) was purchased from Shanghai Macklin Biochemical Co., Ltd. Distilled water was deionized by a MilliQ Water System (18.2 MΩ·cm, Millipore Co., USA).

4.2. Synthesis of colloidal Au NSs

Gold colloid was synthesized by reducing chloroauric acid with sodium citrate, as presented by Frens [42]. Briefly, HAuCl4 solution (0.367 mM, 150 mL) in a 250 mL of round-bottom flask was firstly heated to vigorous boiling, upon the magnetic stirring, 5.25 mL of sodium citrate (1%, m/v) was rapidly added into the solution. The color of the solution changed from pale yellow into black quickly. The mixture was further refluxed for another 15 min until it became a steady, ruby-red suspension. Finally, the suspension was slowly cooled to room temperature and stored at 4 °C for further use.

4.3. Characterization

The size and morphology of Au NSs was measured by transmission electron microscopy (TEM), Tecnai G2SpiritBiotwin (USA). To prepare TEM samples, 10 μL gold colloidal was dropped onto a copper grid, dried up in the air. The UV-Vis spectra of Au NSs and other solutions were measured by a UV-Vis spectrophotometer (Varian InC., USA).

4.4. Detection of Hg^{2+} using PADS

For each measurement, 5.6 μL of MPBA (1 mM) and 56 μL of Hg^{2+} solution (100 pM–10μM) were mixed in a 1.5 mL centrifuge tube to control the final MPBA concentration at 10 μM [36]. All the solutions were transferred using Eppendorf Research plus Single-Channel Pipette (100–1000 μL) and Pipette (20–200 μL). The absorption difference between MPBA-Au NSs solution and Au NSs reached its maximum at the MPBA final concentration of 10 μM. A citric acid/sodium citrate buffer was added into the above mixture to adjust the pH value to 4.0. Then the whole mixture was transferred to the miniature PA cell. After that, 500 mL collidal Au NSs were added in PA cell to keep final MPBA concentration at 10 μM in the mixture, which was considered as best reaction concentration. All solution were mixed at room temperature. The mixed solutions were measured by PADS after 1 min of adding Au NSs. The total operation time was less than 3 min. Each effective PA value was averaged of 5 test values.

Acknowledgments

This work was financially supported by the National Natural Science Foundation of China under grant 61873168 and grant 61503246, and the China Scholarship Council (CSC) Scholarship.

Contributions

All authors made contribution to certain step in the experiment, including setup design, solution formulation and data analysis. Qiaozhi He, Wei Tao and Wenwu Cao were responsible for writing this manuscript. All of the authors gave approval to the final version of this manuscript.

Appendix A. Supplementary data

Supplementary data to this article can be found online at https://doi.org/10.1016/j.microc.2019.104058.

References

[1] L. Copan, J. Fowles, T. Barreau, N. McGee, Mercury toxicity and contamination of households from the use of skin creams adulterated with mercurous chloride (Calomel), Int. J. Environ. Res. Public Health 12 (9) (2015) 10943–10954.
[2] M. Korbas, J.L. O'Donoghue, G.E. Watson, I.J. Pickering, S.P. Singh, G.J. Myers, T.W. Clarkson, G.N. George, The chemical nature of mercury in human brain following poisoning or environmental exposure, ACS Chem. Neurosci. 1 (12) (2010) 810–818.
[3] Y. Zhou, V.S. Vaidya, R.P. Brown, J. Zhang, B.A. Rosenzweig, K.L. Thompson, T.J. Miller, J.V. Bonventre, P.L. Goering, Comparison of kidney injury molecule-1 and other nephrotoxicity biomarkers in urine and kidney following acute exposure to gentamicin, mercury, and chromium, Toxicol. Sci. 101 (1) (2007) 159–170.
[4] A.L.V. Milioni, B.V. Nagy, A.L.A. Moura, E.C. Zachi, M.T. Barboni, D.F. Ventura, Neurotoxic impact of mercury on the central nervous system evaluated by neuropsychological tests and on the autonomic nervous system evaluated by dynamic pupillometry, NeuroToxicology 59 (2017) 263–269.
[5] K. Das, U. Siebert, A. Gillet, A. Dupont, C. Di-Poï, S. Fonfara, G. Mazzucchelli, E. De Pauw, M.-C. De Pauw-Gillet, Mercury immune toxicity in harbour seals: links to in vitro toxicity, Environ. Health 7 (1) (2008) 52.
[6] S.W. Tan, J.C. Meiller, K.R. Mahaffey, The endocrine effects of mercury in humans and wildlife, Crit. Rev. Toxicol. 39 (3) (2009) 228–269.
[7] World Health Organization, Guidelines for Drinking-water Quality, vol. 1, World Health Organization, 2004.
[8] Y. Zhao, J. Zheng, L. Fang, Q. Lin, Y. Wu, Z. Xue, F. Fu, Speciation analysis of mercury in natural water and fish samples by using capillary electrophoresis-inductively coupled plasma mass spectrometry, Talanta 89 (2012) 280–285.
[9] P. Li, X. Feng, G. Qiu, L. Shang, Z. Li, Mercury pollution in Asia: a review of the contaminated sites, J. Hazard. Mater. 168 (2-3) (2009) 591–601.
[10] P. She, Y. Chu, C. Liu, X. Guo, K. Zhao, J. Li, H. Du, X. Zhang, H. Wang, A. Deng, A competitive immunoassay for ultrasensitive detection of Hg2+ in water, human serum and urine samples using immunochromatographic test based on surface-enhanced Raman scattering, Anal. Chim. Acta 906 (2016) 139–147.
[11] C.-W. Liu, C.-C. Huang, H.-T. Chang, Highly selective DNA-based sensor for lead (II) and mercury (II) ions, Anal. Chem. 81 (6) (2009) 2383–2387.
[12] Y. Zhang, G.M. Zeng, L. Tang, J. Chen, Y. Zhu, X.X. He, Y. He, Electrochemical sensor based on electrodeposited graphene-Au modified electrode and nanoAu

carrier amplified signal strategy for attomolar mercury detection, Anal. Chem. 87 (2) (2015) 989–996.
[13] Q. Wang, X. Yang, X. Yang, P. Liu, K. Wang, J. Huang, J. Liu, C. Song, J. Wang, Colorimetric detection of mercury ion based on unmodified gold nanoparticles and target-triggered hybridization chain reaction amplification, Spectrochim. Acta A Mol. Biomol. Spectrosc. 136 (2015) 283–287.
[14] C. Wang, L. Xu, Y. Wang, D. Zhang, X. Shi, F. Dong, K. Yu, Q. Lin, B. Yang, Fluorescent silver nanoclusters as effective probes for highly selective detection of mercury (II) at parts-per-billion levels, Chem. Asian J. 7 (7) (2012) 1652–1656.
[15] L. Zhang, H. Chang, A. Hirata, H. Wu, Q.-K. Xue, M. Chen, Nanoporous gold based optical sensor for sub-ppt detection of mercury ions, Acs Nano 7 (5) (2013) 4595–4600.
[16] K. Saha, S.S. Agasti, C. Kim, X. Li, V.M. Rotello, Gold nanoparticles in chemical and biological sensing, Chem. Rev. 112 (5) (2012) 2739–2779.
[17] W.G. Kreyling, A.M. Abdelmonem, Z. Ali, F. Alves, M. Geiser, N. Haberl, R. Hartmann, S. Hirn, D.J. De Aberasturi, K. Kantner, In vivo integrity of polymer-coated gold nanoparticles, Nat. Nanotechnol. 10 (7) (2015) 619.
[18] W. Zhou, X. Gao, D. Liu, X. Chen, Gold nanoparticles for in vitro diagnostics, Chem. Rev. 115 (19) (2015) 10575–10636.
[19] S. Liu, Z. Du, P. Li, F. Li, Sensitive colorimetric visualization of dihydronicotinamide adenine dinucleotide based on anti-aggregation of gold nanoparticles via boronic acid-diol binding, Biosens. Bioelectron. 35 (1) (2012) 443–446.
[20] Z.F. Gao, W.W. Song, H.Q. Luo, N.B. Li, Detection of mercury ions (II) based on non-cross-linking aggregation of double-stranded DNA modified gold nanoparticles by resonance Rayleigh scattering method, Biosens. Bioelectron. 65 (2015) 360–365.
[21] L. Yang, W. Yun, Y. Chen, H. Wu, X. Liu, M. Fu, Y. Huang, Ultrasensitive colorimetric and fluorometric detection of Hg (II) based on the use of gold nanoparticles and a catalytic hairpin assembly, Microchim. Acta 184 (12) (2017) 4741–4747.
[22] G. Sener, L. Uzun, A. Denizli, Lysine-promoted colorimetric response of gold nanoparticles: a simple assay for ultrasensitive mercury (II) detection, Anal. Chem. 86 (1) (2013) 514–520.
[23] K. Pu, A.J. Shuhendler, J.V. Jokerst, J. Mei, S.S. Gambhir, Z. Bao, J. Rao, Semiconducting polymer nanoparticles as photoacoustic molecular imaging probes in living mice, Nat. Nanotechnol. 9 (3) (2014) 233.
[24] J. Zhong, L. Wen, S. Yang, L. Xiang, Q. Chen, D. Xing, Imaging-guided high-efficient photoacoustic tumor therapy with targeting gold nanorods, Nanomedicine 11 (6) (2015) 1499–1509.
[25] J. Breguet, J.-P. Pellaux, N. Gisin, Photoacoustic detection of trace gases with an optical microphone, Sensors Actuators A Phys. 48 (1) (1995) 29–35.
[26] S. Zhao, W. Tao, Q. He, H. Zhao, H. Yang, Glucose solution determination based on liquid photoacoustic resonance, Appl. Opt. 56 (2) (2017) 193–199.
[27] S. Zhao, W. Tao, Q. He, H. Zhao, W. Cao, A non-invasive photoacoustic and ultrasonic method for the measurement of glucose solution concentration, AIP Adv. 7 (3) (2017) 035313.
[28] K. Rao, A. Chaudhary, F. Yehya, Investigation of solid carbon blacks using pulsed photoacoustic and double resonant Raman spectroscopy for the identification of trinitrotoluene, Sensors Actuators B Chem. 231 (2016) 830–836.
[29] Y. Huang, F. Li, G. Ma, W. Yang, X. Zhang, J. Lin, Y. Luo, P. Huang, Aggregation induced photoacoustic detection of mercury (âĚą) ions using quaternary ammonium group-capped gold nanorods, Talanta 187 (2018) 65–72.
[30] H. Lai, K. Young, Theory of the pulsed optoacoustic technique, J. Acoust. Soc. Am. 72 (6) (1982) 2000–2007.
[31] S.-H. Yoon, Y.-H. Lee, S.-W. Lee, C. Lee, Energy-harvesting characteristics of PZT-5A under gunfire shock, Mater. Lett. 62 (21-22) (2008) 3632–3635.
[32] P. Patimisco, G. Scamarcio, F.K. Tittel, V. Spagnolo, Quartz-enhanced photoacoustic spectroscopy: a review, Sensors 14 (4) (2014) 6165–6206.
[33] W. Li, X. Chen, Gold nanoparticles for photoacoustic imaging, Nanomedicine 10 (2) (2015) 299–320.
[34] A.L. Korich, P.M. Iovine, Boroxine chemistry and applications: a perspective, Dalton Trans. 39 (6) (2010) 1423–1431.
[35] D. Liu, W. Qu, W. Chen, W. Zhang, Z. Wang, X. Jiang, Highly sensitive, colorimetric detection of mercury (II) in aqueous media by quaternary ammonium group-capped gold nanoparticles at room temperature, Anal. Chem. 82 (23) (2010) 9606–9610.
[36] Y. Zhou, H. Dong, L. Liu, M. Li, K. Xiao, M. Xu, Selective and sensitive colorimetric sensor of mercury (II) based on gold nanoparticles and 4-mercaptophenylboronic acid, Sensors Actuators B Chem. 196 (2014) 106–111.
[37] A.C. Tam, Applications of photoacoustic sensing techniques, Rev. Mod. Phys. 58 (2) (1986) 381–431.
[38] P.W. Ayers, The physical basis of the hard/soft acid/base principle, Faraday Discuss. 135 (2007) 161–190.
[39] G.-H. Chen, W.-Y. Chen, Y.-C. Yen, C.-W. Wang, H.-T. Chang, C.-F. Chen, Detection of mercury (II) ions using colorimetric gold nanoparticles on paper-based analytical devices, Anal. Chem. 86 (14) (2014) 6843–6849.
[40] B.-C. Ye, B.-C. Yin, Highly sensitive detection of mercury (II) ions by fluorescence polarization enhanced by gold nanoparticles, Angew. Chem. Int. Ed. 47 (44) (2008) 8386–8389.
[41] C.-W. Liu, Y.-T. Hsieh, C.-C. Huang, Z.-H. Lin, H.-T. Chang, Detection of mercury (II) based on Hg 2+-DNA complexes inducing the aggregation of gold nanoparticles, Chem. Commun. (19) (2008) 2242–2244.
[42] G. Frens, Controlled nucleation for the regulation of the particle size in monodisperse gold suspensions, Nat. Phys. Sci. 241 (105) (1973) 20.